Chapter 10
Phonon Interference and Energy Transport in Nonlinear Lattices with Resonance Defects

Yuriy A. Kosevich, Haoxue Han, Lyudmila G. Potyomina, Alexandre N. Darinskii and Sebastian Volz

Abstract We introduce and model a three-dimensional atomic-scale phononic metamaterial producing two-path interference phonon antiresonances to control the heat flux spectrum. We show that a crystal plane partially filled with defect-atom arrays causes a total phonon reflection at the frequencies determined by masses and interaction forces. Such patterned atomic planes can be considered as high-finesse atomic-scale interference phonon metamirrors. We emphasize the predominant role of the second phonon path and destructive interference in the origin of the total reflection in comparison with the Fano-resonance concept. The random defect distribution in the plane and the anharmonicity of interatomic bonds do not deteriorate the interference antiresonances. The width of the interference antiresonance dip can provide a measure of the coherence length of the phonon wave packet. All our conclusions

Yu.A. Kosevich (✉)
Semenov Institute of Chemical Physics, Russian Academy of Sciences,
4 Kosygin Street, Moscow 119991, Russia
e-mail: yukosevich@gmail.com

H. Han · S. Volz
CNRS, UPR 288 Laboratoire D'Energétique Moléculaire et Macroscopique,
Combustion (EM2C) and Ecole Centrale Paris, Grande Voie des Vignes,
Châtenay-Malabry 92295, France
e-mail: haoxue.han@ecp.fr

S. Volz
e-mail: sebastian.volz@ecp.fr

L.G. Potyomina
Department of Physics and Technology, National Technical University
"Kharkiv Polytechnic Institute", 21 Frunze Street, Kharkiv 61002, Ukraine
e-mail: potyomina@kpi.kharkov.ua

A.N. Darinskii
Institute of Crystallography, Russian Academy of Sciences,
59 Leninskii Avenue, Moscow 119333, Russia
e-mail: alexandre_dar@mail.ru

J.F.R. Archilla et al. (eds.), *Quodons in Mica*, Springer Series
in Materials Science 221, DOI 10.1007/978-3-319-21045-2_10

are confirmed both by analytical studies of the equivalent quasi-one-dimensional lattice models and by numerical molecular dynamics simulations of realistic lattices in three dimensions.

10.1 Introduction

We provide a new approach to demonstrate that heat in solids can be manipulated like light. While heat convection by fluids and heat radiation by light can be reasonably controlled, the conduction of heat through solids is less straightforward and has been an important challenge both in physics and engineering. Heat at room temperature is carried by lattice vibrations of ultra-high frequencies (10^{12} Hz), which are also called phonons, the quasi-particles that are analogous to the photons that carry light. In this work, we precisely control the heat flow by the *atomic-scale phononic metamaterial*, which contains deliberate flaws in the crystalline atomic lattice, channeling the heat through different phonon paths. Destructive interference between heat waves following different paths leads to the total reflection of the heat current and thus to the remarkable reduction in the material ability to conduct heat. By exploiting this destructive phonon interference, we model a very counter-intuitive possibility of thermal transport: more heat flow is blocked by the opening of the additional phonon channels. We provide an important further insight into the coherent control of phonons which can be applied both to sound and heat propagation.

Destructive interference between waves propagating across laterally inhomogeneous interface layer can result in their total reflection. For instance, the strong resonance electromagnetic reflection found in metafilms partially filled with asymmetrical split-ring arrays [11], in flexible metasurfaces [45] and in stereometamaterials [31] has offered the prospect of a multitude of applications as quantum optics [1] and negative refraction [13]. As another example of destructive interference in optics, two-photon interference can result in a total cancellation of the photon output because of the coalescence of the two single photons, which was first observed by Hong et al. [18]. This interference effect occurs because two possible photon paths interfere destructively, which produces the famous Hong-Ou-Mandel (HOM) dip in the detection probability of the output photons. The HOM dip has since been demonstrated both in optical [3, 40] and microwave [46] regimes. Recently the two-photon destructive interference was demonstrated in a three-dimensional (3D) optical metamaterial [29].

Similar destructive interference effect which results in the total reflection can be also realized in a phonon system. For sound waves, the enhanced phonon reflection was first described in [22] and [12] independently. Reference [22] interpreted the anomalous reflection of a long acoustic wave by a two-dimensional (2D) crystal defect as the *destructive interference between two phonon paths*: through the nearest-neighbor bonds and through the non-nearest-neighbor bonds which couple directly atomic layers adjacent to the defect plane. Reference [12] drew an analogy between electron scattering and phonon scattering and calculated numerically the phonon

transmission with an asymmetric profile through a strip of oscillator chains connected in parallel.

Constant endeavor has been devoted to the precise control of heat conduction. Recent efforts have been concentrated on reducing the thermal conductivity κ via nanostructured materials with superlattices [5, 7, 21] and with embedded nanoparticles [6, 34, 37]. Most works have attributed the reduction in κ to the increased phonon scattering rate and the decreased phonon mean free path (MFP), which corresponds to the particle description of thermal transport in a lattice. However, the role of the destructive phonon interference is not well understood in the tailoring of thermal transport in the wave picture. Thermal conductivity is a physical phenomenon that requires phonon anharmonicity as a key ingredient. In a perfect insulating crystal, harmonic phonons would never be scattered and such a crystal would have anomalous, diverging with the crystal size, thermal conductivity at all temperatures. Scattering of phonons by lattice imperfections, e.g., by isotopic impurities, in a one-dimensional (1D) crystal also does not result in the normal, converging with the crystal length, thermal conductivity [4, 39]. Only anharmonic phonon-phonon interactions and scattering can result in the normal heat transport in low-dimensional crystals, and there is a great variety of nonlinear interatomic potentials which lead either to the normal or anomalous heat transport in one-dimensional chains [41]. Here we implement large-scale molecular dynamics (MD) simulations of phonon wave packet propagation in 3D lattices that incorporate realistic lattice potentials, which properly account for the nonlinearities in the interatomic interactions. Our MD simulations of anomalous phonon reflection (interference antiresonances) of short-wavelength phonons from internal crystal plane with embedded defects in a 3D lattice confirm previous analytical results for anomalous reflection of long-wavelength phonons in a 3D crystal with planar distribution of resonance defects (with 2D planar resonance defect) [22, 26] and of finite-wavelength phonons in 1D atomic chain with resonance defects [23, 24]. In addition to the results on anomalous phonon scattering in harmonic lattices with resonance defects, we also show that the two-path interference antiresonances remain pronounced even when the interaction nonlinearity becomes fairly strong in a real 3D lattice. Therefore the two-path phonon interference in the proposed phononic metamaterial makes it possible to control thermal energy transport even in the case of large-amplitude lattice vibrations, for instance at room and higher temperature.

10.2 Model Structures and Simulation Methodology

Here we introduce and model a realistic 3D atomic-scale phononic metamaterial which can be used for the storage and lasing of coherent terahertz phonons and for manipulating the flow of thermal energy [15, 16]. Phonon reflection is generated by exploiting the two-path phonon interference on internal crystal planes with embedded defects. The 2D planar defects force phonons to propagate through the two paths: through unperturbed (matrix) and perturbed (defect) interatomic bonds [22–24]. The

resulting phonon interference gives antiresonances (zero-transmission resonances) in the phonon transmission spectra that can be controlled by the masses, force constants and 2D concentration of the defect atoms. Such patterned atomic planes can be considered as high-finesse atomic-scale *interference phonon metamirrors*. Our results show that the patterning of the defect-atom arrays with the formation of phonon metamirrors can lead to a new departure in thermal energy management [33], offering potential applications in thermal filters [48], thermal diodes [30] and thermal cloaking [17, 36, 47].

10.2.1 Model Structure

Atomic distribution in the 3D phononic metamaterial with a face-centered cubic (FCC) lattice with a 2D array of heavy defect atoms is depicted in Fig. 10.1a. Each interference phonon metamirror consists of an atomic-scale metafilm: an internal (001) crystal plane in a cubic silicon (Si) lattice partially filled with germanium (Ge) impurity atoms, as shown in Fig. 10.1a. The defect atoms can be distributed periodically or randomly in the defect crystal plane with different filling fractions f_d. When the defects do not fill completely the defect plane, phonons have two paths to cross such an atom array as shown in Fig. 10.1a, whereas the phonon path through the host atoms is blocked when the defect layer is constituted by a uniform impurity-atom array, 100 % packed with the impurity atoms. Two types of atomic-scale metamaterials were studied using realistic interatomic potentials: a FCC lattice of argon (Ar), in which the defects are heavy Ar isotopes, and a diamond lattice of silicon with germanium atoms as the heavy-mass and atomic-bonds defects.

10.2.2 Methodology

The interactions between Ar atoms are described by the Lennard-Jones potential [19]. The covalent Si:Si/Ge:Ge/Si:Ge interactions are modeled by the Stillinger-Weber potential [44]. To probe the phonon transmission, MD with the phonon wave packet method [43] was used to provide the per-phonon-mode energy transmission coefficient $\alpha(\omega, l)$. We excited a realistic 3D Gaussian wave packet centered at the frequency ω and wave vector $\mathbf{k}$ in the reciprocal space and at $\mathbf{r}_0$ in the real space, with the spatial width (coherence length) l in the direction of $\mathbf{k}$. The wave packet generation was performed by assigning the displacement $\mathbf{u}_i$ for the atom i as:

$$\mathbf{u}_i = A\mathbf{e}_i(\mathbf{k}) \exp\left(\mathrm{i}\left[\mathbf{k}\cdot(\mathbf{r}_i - \mathbf{r}_0) - \omega t\right]\right) \exp\left(-\frac{\left[\mathbf{r}_i - \mathbf{r}_0 - \mathbf{v}_g t\right]^2}{4l^2}\right), \qquad (10.1)$$

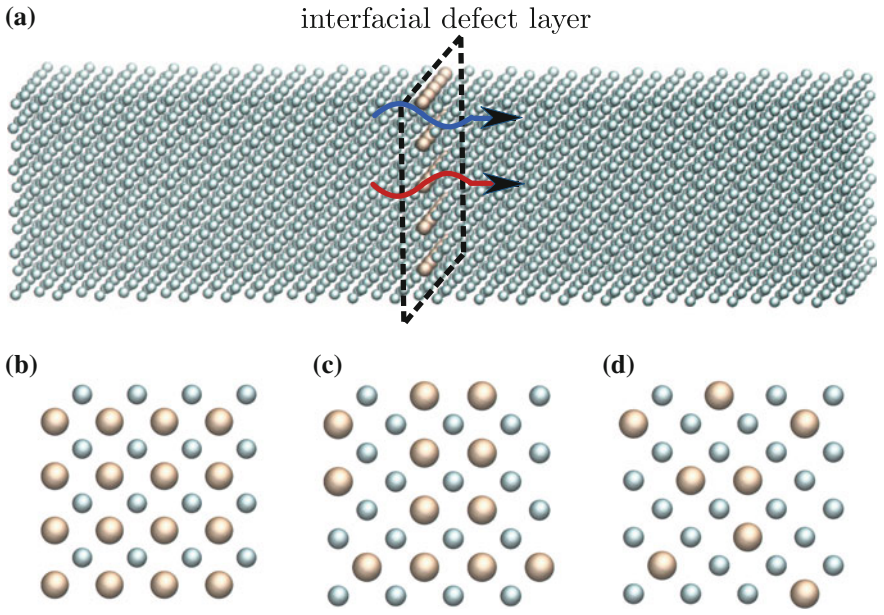

Fig. 10.1 (color online). **a** Interference Phonon Metamirror: 3D face-centered cubic lattice containing an internal (001) crystal plane in which an impurity-atom array is embedded. The *brown* atoms are the defect atoms and the *green* ones are the atoms of the host lattice. The *red* and *blue curves* refer to the phonon paths through the impurity atom bonds and through the host atom bonds, respectively. The presence of the two possible phonon paths can result in the two-path destructive-interference transmission antiresonance. **b** Periodic distribution of defect atoms with filling fraction $f_d = 50\,\%$. Randomly distributed defect atoms with **c** $f_d = 37.5\,\%$ and **d** $f_d = 25\,\%$

where A is the wave packet amplitude, $\mathbf{e}_i(\mathbf{k})$ is the phonon polarization vector, ω is the eigenfrequency for the wave vector $\mathbf{k}$ within a single branch of the phonon dispersion curve, $\mathbf{v}_g$ is the phonon group velocity along the wave vector $\mathbf{k}$ at the wave packet center frequency ω. Wave amplitude A of the generated phonon wave packets was taken sufficiently small such that the anharmonic coupling to other lattice modes is kept weak. Hence the wave packets propagate in an effectively harmonic crystal without any perceptible spreading or scattering. The wave packet was set to propagate normally to the defect layer, where an elastic scattering results in transmitted and reflected waves. The wave packet energy transmission coefficient $\alpha(\omega, l)$ is defined as the ratio between the energy carried by the transmitted and initial wave packets, centered at the given phonon mode $(\omega, \mathbf{k})$ with the spatial extent l. The plane-wave limit is reproduced by the wave packets with the spatial width l much larger than the wavelength λ_c of the wave packet central frequency. All the MD simulations were performed with the LAMMPS code package [27, 38].

10.3 Results and Discussions

In this section we consider separately the interference resonance profile in the phonon transmission coefficient, the isotopic shift of the resonance reflection versus the defect masses, and the phonon screening effect in the thermal conductance. Then we report the two-path phonon interference in a silicon crystal with germanium impurities. We show that the random distribution of the defects in the crystal plane and the nonlinearity of the potential do not deteriorate the interference resonances. Finally we show that the width of the interference antiresonance dip can provide a measure for the coherence length of the phonon wave packet.

10.3.1 Interference Resonance Profile

The transmission coefficient $\alpha(\omega)$ of the wave packet with $l = 20\lambda_c$, retrieved from MD simulations of an Ar metamaterial, is presented in Fig. 10.2. The incident phonons undergo a total reflection from the defect layer at the antiresonance frequency ω_R. Phonon transmission spectra displays an interference antiresonance profile since the two phonon paths interfere destructively at ω_R. A total transmission at ω_T follows the interference antiresonance, which is reminiscent of the Fano resonances [10]. For a uniform heavy-defect-atom array, the zero-transmission antiresonance profile will be totally suppressed and replaced by a monotonous decay of the transmission with frequency. In the latter case, only the phonon path through the defect atoms is accessible.

We emphasize that the second phonon path is indispensable to the emergence of the zero-transmission dip, which cannot be sufficiently described by the Fano resonance. We clarify this by studying the phonon transmission across two successive internal crystal planes completely filled with resonance heavy impurity atoms, when a local resonant transmission maximum is observed instead of a zero-transmission dip, see Fig. 4a in [23] and Fig. 2 in [16]. This transmission maximum satisfies well the Fano-resonance condition [10] of a discrete state resonating with its continuum background, but no zero-transmission dip occurs because of the absence of the second phonon path [22, 26]. This transmission maximum can be considered as a phonon analogue of the Fabry-Pérot resonance in optics, which requires only a single phonon (or photon) path. Therefore this observation clearly corroborates the two-path destructive phonon interference nature of the zero-transmission dip (antiresonance) in the phonon transmission coefficient $\alpha(\omega)$.

To understand further the phonon antiresonances caused by the interference between two phonon channels, we use an equivalent model of monatomic quasi-1D lattice of coupled harmonic oscillators [23], depicted in the inset in Fig. 10.2. In model (a), phonons propagate through the two paths: through the host atom bonds, and through those of the impurity atoms, whereas in model (b) only the second chan-

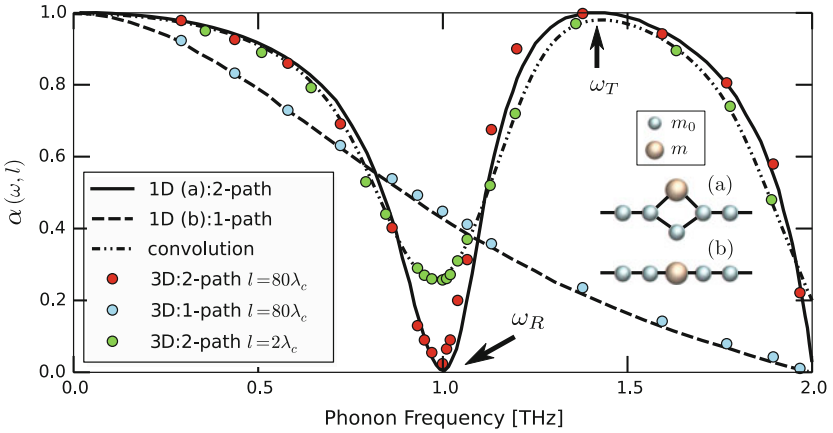

Fig. 10.2 (color online). Spectra of the energy transmission coefficient $\alpha(\omega, l)$ predicted by equivalent quasi-1D model (*solid* and *dashed lines*) and by MD simulations (*symbols*) for a 3D Ar metamaterial with defect crystal plane containing heavy isotope impurities, with mass $m = 3m_0$. *Dashed-dotted line* is the convolution (10.3) of the plane-wave transmission coefficient $\alpha(\omega)$ from (10.2) with a Gaussian wave packet in frequency domain with $l = 2\lambda_c$. *Red* and *blue symbols* present transmission of the wave packet with $l = 20\lambda_c$ through the two paths and through one path in the Ar metamaterial with planar defect, respectively; *green symbols* present transmission of the wave packet with $l = 2\lambda_c$ through the two paths. *Inset:* Two possible quasi-1D lattice models describing phonon propagation through the lattice region containing the local defect: **a** phonons can propagate through the defect and host atoms bonds; **b** phonons can propagate only through the defect atom bonds. *Black sticks* between the atoms present atom bonds. In the case of Ar lattice, the coefficients in (10.2) are $\omega_R = 1.0$, $\omega_T = 1.4$, $\omega_{max} = 2.0$ and $C = 0.25$. The quasi-1D model (**a**) is equivalent to a 2D crystal plane partially filled with periodically alternating isotopes with different masses, with $f_d = 50\,\%$, in a 3D Ar lattice. The 1D model (**b**) is equivalent to a 2D crystal plane completely filled with heavy isotopes, with $f_d = 100\,\%$, in a 3D Ar lattice

nel remains open. The model (a) gives the energy transmission coefficient for the plane wave:

$$\alpha(\omega) = \frac{(\omega^2 - \omega_R^2)^2(\omega_{max}^2 - \omega^2)}{(\omega^2 - \omega_R^2)^2(\omega_{max}^2 - \omega^2) + C\omega^2(\omega^2 - \omega_T^2)^2}\,, \tag{10.2}$$

where $\omega_{R,T}$ are the frequencies of the reflection and transmission resonances, ω_{max} is the maximal phonon frequency for a given polarization, $\omega_R < \omega_T < \omega_{max}$. C is a real positive coefficient given by the atomic masses, force constants and f_d, $C = 0$ for $f_d = 0$. The ω_R frequency exists only in the presence of the additional channel, which is open for wave propagation through the bypath around the defect atom, see inset (a) in Fig. 10.2. As follows from (10.2) and Fig. 10.2, $\alpha(\omega_R) = \alpha(\omega_{max}) = 0$ and $\alpha(0) = \alpha(\omega_T) = 1$.

The energy transmission coefficient $\alpha(\omega, l)$ of the wave packet with the given central frequency ω and spatial width l is determined by the convolution of the transmission coefficient for the plane wave $\alpha(\omega) = \alpha(\omega, \infty)$, given by (10.2), with

a Gaussian wave packet in frequency domain with the width $\Delta\omega = v_g/(2l)$:

$$\alpha(\omega, l) = \int_{-\omega_{max}}^{\omega_{max}} \alpha(\omega') \exp\left(-\frac{(\omega-\omega')^2}{2\Delta\omega^2}\right) \frac{d\omega'}{\Delta\omega\sqrt{2\pi}}. \tag{10.3}$$

It is noteworthy that the Gaussian phonon wave packets minimize the product of the frequency, $\Delta\omega$, and time, $\Delta t = l/v_g$, uncertainties: $\Delta\omega \cdot \Delta t = 1/2$, as well as the product of the wave number component, $\Delta k_x = \Delta\omega/v_g = 1/(2l)$, and coordinate, $\Delta x = l$, uncertainties: $\Delta k_x \cdot \Delta x = 1/2$, see also Sect. 10.3.7. This property of the Gaussian phonon wave packets is similar to the property of the Gaussian wave packets of coherent states in quantum mechanics, which minimize the product of the momentum component, Δp_x, and coordinate uncertainties: $\Delta p_x \cdot \Delta x = \hbar/2$ [28], see also [25] for a similar property of the Gaussian wave packets of magnon coherent states in spin chains.

In the transmission of a narrow wave packet with $l = 2\lambda_c$, the interference effect is weakened by a large number of frequency components, when the plane-wave approximation ($l \gg \lambda_c$) is broken and the transmission at ω_R is not zero any more, i.e. $\alpha(\omega_R, l) > 0$, which is the case also in [18]. As one can see in Fig. 10.2, an excellent agreement in transmission coefficients is demonstrated between the equivalent quasi-1D model provided by (10.2) and (10.3) and the MD simulations of the 3D atomic-scale phononic metamaterial with the use of realistic interatomic potentials.

10.3.2 Isotopic Shift of Resonances

In a lattice with atomic impurities, the substituent atoms scatter phonons due to the difference in mass and/or bond stiffness. Since no bond defect was introduced, the loci of the resonances are determined only by the mass ratio (MR) of the isotope defects and host atoms. As the isotope defects become heavier, the two-path phonon interference antiresonance becomes more pronounced in terms of the depth and width of the phonon-transmission dip and demonstrates a red-shift of the dip, thus impeding the long-wavelength phonons, as shown in Fig. 10.3a, c for longitudinal and transverse phonons, respectively. The equivalent quasi-1D lattice model gives the following expression for the frequency of the transmission dip:

$$\omega_R = \omega_{max}/\sqrt{m/m_0 + 1}, \tag{10.4}$$

where m and m_0 refer to the atomic mass of the isotope defect and host atom, with MR $= m/m_0 > 1$. The transmission resonance at $\omega = \omega_T$ is much less sensitive to the defect mass since it is largely determined by the mass of the host atom. As depicted in Fig. 10.3b, d, the spectral positions of the interference resonances ω_R

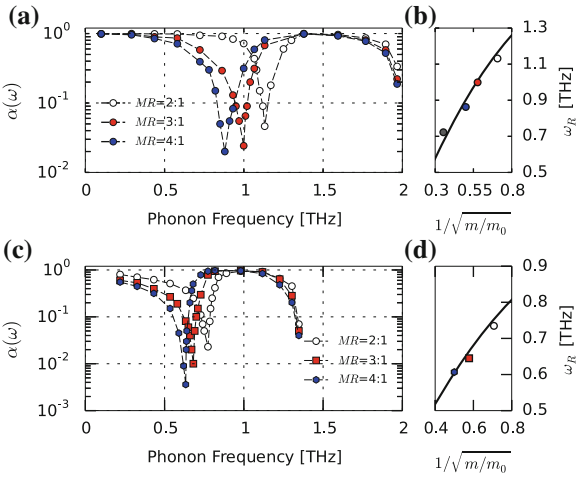

Fig. 10.3 (color online). **a** and **c**: Spectra of phonon transmission coefficient $\alpha(\omega)$ of longitudinal (**a**) and transverse (**c**) acoustic waves through the phononic metamaterial, which consists of 2D crystal plane filled with periodically alternating isotopes with different mass ratio (MR) m/m_0, with $f_d = 50\,\%$ in a 3D Ar lattice. *Dashed lines* are the guides to the eye. **b** and **d**: Isotopic shift of the two-path phonon interference antiresonance versus the inverse square root of the mass ratio for longitudinal (**b**) and transverse (**d**) acoustic waves. *Symbols* present the resonances predicted by MD simulations for a 3D lattice, *solid line* shows the analytical prediction of the equivalent quasi-1D lattice model given by (10.4)

are again in an excellent agreement with the analytical prediction of the equivalent quasi-1D lattice model given by (10.4) for both longitudinal and transverse phonons.

10.3.3 Phonon Screening Effect

In Fig. 10.2, the transmission spectra for longitudinal phonons across the uniform defect-atom array is plotted to be compared with that of the 50 %-filled defect-atom array. At the frequency of the two-path interference antiresonance ω_R, an array of 50 % defect atoms has a transmittance two orders of magnitude smaller than that of a uniform defect-atom array. The difference between the very strong phonon reflection by a 50 %-filled defect array and the high phonon transmission across a uniform defect array can result in a counter-intuitive effect: an array of randomly alternating host and impurity atoms can scatter more phonons than an array with a uniform distribution of heavy isotopes. This anomalous phonon reflection phenomenon in molecular systems can find its acoustic counterpart in macroscopic structures [9, 23, 32]. In [9], perforated plates were proved to shield ultrasonic acoustic waves in water much more effectively than uniform plates. Liu et al. [32] managed to break the mass-density law for sonic transmission by embedding high-density spheres coated

with a soft material in a single layer of a stiff matrix. We calculate the interfacial thermal conductance G by following the Landauer-like formalism [20]:

$$G = \int \sum_{\nu} \hbar\omega(\mathbf{k}, \nu) v_{g,z}(\mathbf{k}, \nu) \alpha \frac{\partial}{\partial T} n_{\mathrm{BE}}(\omega, T) \frac{\mathrm{d}\mathbf{k}}{(2\pi)^3}, \tag{10.5}$$

where $\hbar$ is the reduced Planck constant, $v_{g,z}$the phonon group velocity in the cross-plane direction, $n_{\mathrm{BE}}(\omega, T)$ is the Bose-Einstein distribution of phonons at temperature T, $n_{\mathrm{BE}}(\omega, T) = [\exp(\hbar\omega/k_B T) - 1]^{-1}$, k_B is the Boltzmann constant. The integral is carried out over the Brillouin zone and the sum is over the phonon branches. By embedding defect atoms in a crystal plane monolayer, we manage to reduce the thermal conductance by 30 % with respect to the case of pristine lattice, with no defects, as shown in Fig. 10.4a. This destructive-interference-induced effect can be used for the explanation of the remarkable decrease of κ of SiGe alloy with very small amount of Ge atoms, with respect to the pristine Si lattice [14]. G is further reduced by considering the (second) non-nearest-neighbor (NNN) bonds C_2 between the host atoms on the two sides of the uniform defect layer in addition to the nearest-neighbor (NN) bond C_1 linking the host and adjacent defect atoms, see also [22, 23]. This reduction comes from the suppression of phonon transmission at high frequencies, shown in Fig. 10.4b, which is due to the opening of the second phonon path through the host atom bonds, destructively interfering with the first path through the defects. The occurrence of the second phonon path substantially reduces G by 16 % even if it is weak: $C_2 = 0.08C_1$. This provides another evidence of the control of heat transport by the two-path destructive phonon interference: more heat flux is blocked despite the opening of the additional phonon paths, even in the absence of phonon resonances.

10.3.4 Two-Path Phonon Interference in Si Crystal with Ge Impurities

Figure 10.5 illustrates the two-path interference phonon antiresonances in the metamaterial fabricated as follows: 2D planar distribution of Ge atoms is embedded in a Si crystal. Ge and Si atoms have mass ratio of 2.57 and thus the Ge-atom array introduces both the heavy-mass and atomic-bond defects due to a weaker Si:Ge coupling than the Si:Si interaction [44]. Phonons from transverse and longitudinal acoustic branches experience strong resonant reflections at the defect crystal plane, 50 %-filled with Ge atoms, while the short-wavelength phonons near the edge of the Brillouin zone are strongly reflected by the defect crystal plane, completely filled with Ge atoms.

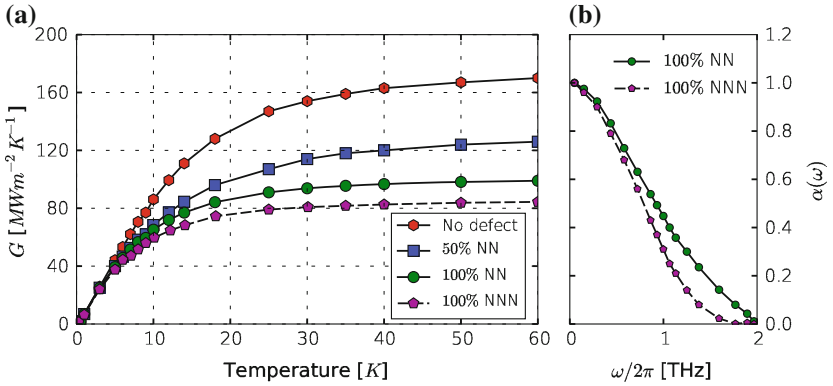

Fig. 10.4 (color online). **a** Temperature dependence of interfacial thermal conductance across a crystal plane, 50 %-filled with periodic array of heavy isotope defects (*rectangles*), and across a uniform defect crystal plane with (*pentagons*) and without (*circles*) the second phonon path induced by the non-nearest-neighbor (NNN) bonds in addition to the nearest-neighbor (NN) bonds, in comparison with that across an atomic crystal plane without defects (*hexagons*). **b** Transmission coefficient $\alpha(\omega)$ through a uniform defect crystal plane with (*pentagons*) and without (*circles*) the second phonon path induced by the NNN bonds

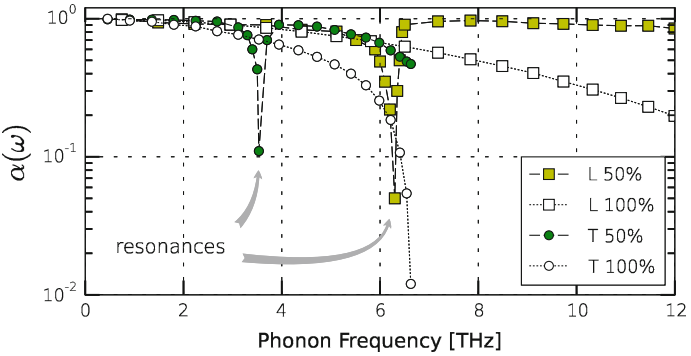

Fig. 10.5 (color online). Two-path interference phonon antiresonances for transverse and longitudinal phonons on a partially-Ge-filled defect crystal plane (*green circles* and *yellow squares*) plotted along with the non-resonant transmission through a completely-Ge-filled defect crystal plane (*open squares* and *circles*) in a Si crystal as phononic metamaterial

10.3.5 Random Distribution of Atoms

In contrast to light [8, 35], even a single defect atom in a crystal plane produces interference reflection antiresonances for Gaussian beams with finite beam diameters of (longitudinal or transverse) phonons because of the presence of the two phonon paths. Therefore, phonon reflection antiresonances should exist even in the absence of the periodicity in the defect-atom distribution in the crystal plane because of the localized nature of the resonances. This argument is supported by further study

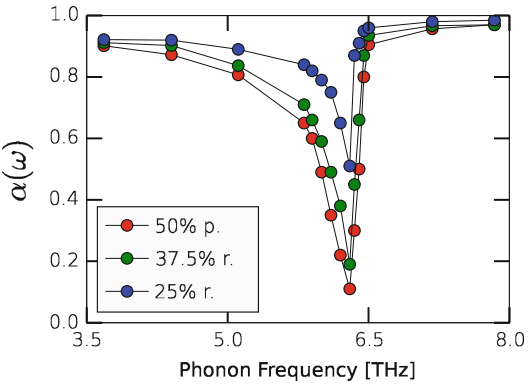

Fig. 10.6 (color online). Transmission coefficient $\alpha(\omega)$ for longitudinal phonons across the planar defect in a Si crystal, which contains randomly (r.) distributed embedded Ge atoms with $f_d = 37.5$ and 25 %, compared with $\alpha(\omega)$ across the planar defect, which contains periodically (p.) distributed embedded Ge atoms with $f_d = 50\,\%$. The computed $\alpha(\omega)$ was averaged over different random distributions

of phonon transmission through the arrays of Ge atoms in a crystal plane in Si-crystal-based phononic metamaterial, distributed with different filling fractions f_d and randomness. Strong transmission dip, similar to that produced by periodic Ge atoms arrays, remains pronounced in both cases, as shown in Fig. 10.6. This was shown experimentally to be equally valid in macroscopic acoustic metamaterials [32].

Chen et al. reduced the thermal conductivity κ below the alloy limit by the partial intermixing (segregation) of Ge atoms in Si superlattices [6]. Their ab initio calculations showed that phonon mean free path was substantially reduced in the low frequencies [6]. We note that the clusters of Ge atoms can be considered as randomly dispersed heavy-mass oscillators, which scatter low-frequency phonons at the interference antiresonances whose frequencies are given by the isotopic-shift law (10.4). With the destructive interference, we can also relate the extremely low κ found in the $In_{0.53}Ga_{0.47}As$ alloy, randomly filled with heavy ErAs nanoparticles [21].

10.3.6 Nonlinear Effects

The nonlinear effects in the two-path interference phonon antiresonances were studied by increasing the amplitude A of the incident phonon wave packet, as shown in Fig. 10.7 for the phonon transmission coefficient through the partially-Ge-filled, with $f_d = 50\,\%$, internal crystal plane in Si lattice. As A increases, the reflection becomes less pronounced with more heat flux passing through, which provides direct evidence of inelastic phonon scattering at the defect plane. The antiresonances demonstrate the red shifts in frequency due to the anharmonic (cubic first of all) terms in the interatomic potential. We also note in this connection that our computation of a

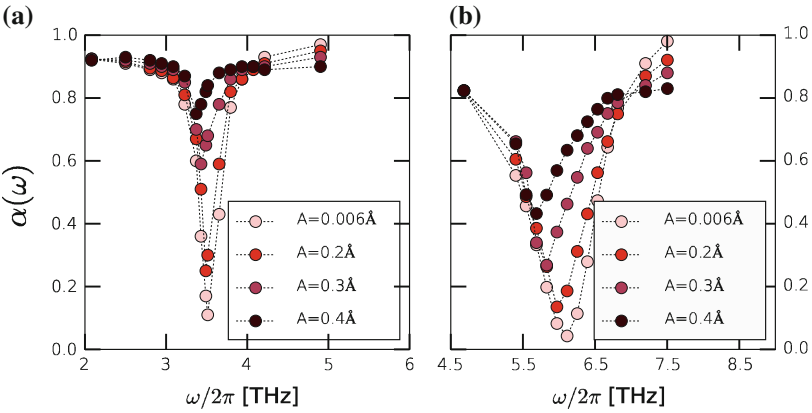

Fig. 10.7 (color online). Evolution of the interference antiresonance in the phonon transmission coefficient $\alpha(\omega)$ through the partially-Ge-filled, with $f_d = 50\,\%$, internal crystal plane in Si lattice versus the increasing wave amplitude for **a** transverse and **b** longitudinal phonons

quasi-1D atomic chain, containing an impurity atom characterized by non-parabolic (nonlinear) interaction potential with the neighboring host atoms, agrees well with our MD results for 3D lattice. The interference antiresonances remain pronounced even when the interaction nonlinearity becomes fairly strong. Therefore the two-path interference phonon antiresonances in the proposed phononic metamaterial make it possible to control thermal energy transport even in the case of large-amplitude lattice vibrations, for instance at room and higher temperature.

10.3.7 Wave Packet Coherence Length Determination

The decrease in 2D defect filling fraction f_d narrows the width of the antiresonance dip because of the weakening of the relative strength of the "defect-bond" phonon paths through the crystal plane, see Fig. 10.1 and (10.2). In general, the width $\Delta\omega$ of the antiresonance dip for the two-path phonon interference is determined by both the f_d and finite coherence length l of the phonon wave packet. As follows from Fig. 10.2, for the large $f_d = 50\,\%$ $\Delta\omega$ is not sensitive to l. In the limit of small f_d and for $l \gg \lambda_c$, $\Delta\omega$ is narrow and proportional to f_d, as shown in Figs. 10.6 and 10.8. In this limit, for the wave packet with a short width $l, l \sim \lambda_c$, $\Delta\omega$ will be determined mainly by l. From Fig. 10.8, the width $\Delta\omega$ of the antiresonance dip for the wave packet with $l = 2\lambda_c$ is $\Delta\omega/(2\pi) = 0.19\,\text{THz}$. Then from the minimal value of the product $\Delta\omega \cdot \Delta t = 1/2$, which is realized for the Gaussian wave packets, we get the wave packet width in time domain $\Delta t = 0.42\,\text{ps}$ and the wave packet spatial width (coherence length) $l = v_g \Delta t \approx 3.1\,\text{nm}$, where $v_g \approx 7.5\,\text{km/s}$ is the longitudinal phonon group velocity in Si at $\omega = \omega_R$, see [42]. This length coincides with the

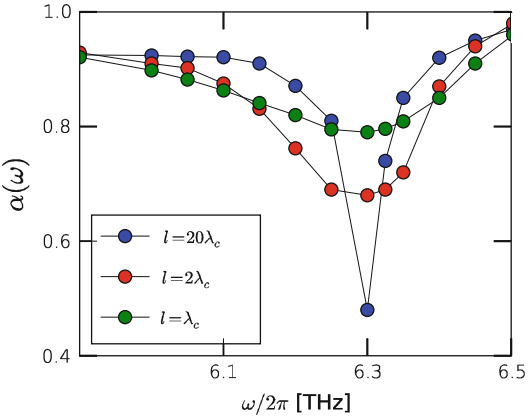

Fig. 10.8 (color online). Broadening of the antiresonance dip in the energy transmission coefficient $\alpha(\omega, l)$ in the limit of small filling fraction $f_d = 5\,\%$ for the wave packets with short coherence lengths ($l = \lambda_c$ and $l = 2\lambda_c$, *green* and *red circles*), in comparison with that for an almost plane-wave wave packet ($l = 20\lambda_c$, *blue circles*)

wave packet coherence length $l \approx 3.2\,\text{nm}$, which was used in the MD simulations shown in Fig. 10.8. The width $\Delta\omega$ of the antiresonance dip for the wave packet with a shorter coherence length $l = \lambda_c$ is larger than that of the wave packet with $l = 2\lambda_c$, see Fig. 10.8. Therefore the width of the two-path phonon interference antiresonance dip in the transmission spectrum can provide a measure of the coherence length of the phonon wave packet.

10.4 Conclusions

In conclusion, we provide a comprehensive modeling of atomic-scale phononic metamaterial for the control of heat transport by exploiting the two-path interference phonon antiresonances. Thermal phonons crossing crystal plane partially filled with resonance defect atoms can undergo complete reflection caused by destructive phonon interference. Such patterned atomic planes can be considered as high-finesse atomic-scale *interference phonon metamirrors*. Interference phonon antiresonances are not deteriorated by the aperiodicity in the defect-atom distribution and the anharmonicity of interatomic bonds. The width of the antiresonance dip provides a measure of the coherence length of the phonon wave packet. And, finally, we would like to emphasize that strong resonance reflections of electromagnetic waves, which have been observed in metafilms partially filled with asymmetrical split-ring arrays [11], in stereometamaterials [31], in flexible metasurfaces [45] and in microwave metamirrors [2], can also be interpreted as *interference photon antiresonances* in an optically transparent plane, partially filled with subwavelength plasmonic or microwave resonating structures [16, 23].

Acknowledgments Yu.A.K. acknowledges the Ecole Centrale Paris and EM2C Laboratory for the hospitality during the stay during which this work was initiated.

References

1. Altewischer, E., Van Exter, M.P., Woerdman, J.P.: Plasmon-assisted transmission of entangled photons. Nature **418**(6895), 304–306 (2002)
2. Asadchy, V.S., Radi, Y., Vehmas, J., Tretyakov, S.A.: Functional metamirrors using bianisotropic elements. Phys. Rev. Lett. **114**(9), 095503 (2015)
3. Beugnon, J., Jones, M.P.A., Dingjan, J., Darquié, B., Messin, G., Browaeys, A., Grangier, P.: Quantum interference between two single photons emitted by independently trapped atoms. Nature **440**(7085), 779–782 (2006)
4. Casher, A., Lebowitz, J.L.: Heat flow in regular and disordered harmonic chains. J. Math. Phys. **12**(8), 1701–1711 (1971)
5. Chen, G., Shakouri, A.: Heat transfer in nanostructures for solid-state energy conversion. Trans. Am. Soc. Mech. Eng. **124**, 242–252 (2002)
6. Chen, P., Katcho, N.A., Feser, J.P., Li, W., Glaser, M., Schmidt, O.G., Cahill, D.G., Mingo, N., Rastelli, A.: Role of surface-segregation-driven intermixing on the thermal transport through planar Si/Ge superlattices. Phys. Rev. Lett. **111**(11), 115901 (2013)
7. Chowdhury, I., Prasher, R., Lofgreen, K., Chrysler, G., Narasimhan, S., Mahajan, R., Koester, D., Alley, R., Venkatasubramanian, R.: On-chip cooling by superlattice-based thin-film thermoelectrics. Nature Nanotechnol. **4**(4), 235–238 (2009)
8. Degiron, A., Lezec, H.J., Yamamoto, N., Ebbesen, T.W.: Optical transmission properties of a single subwavelength aperture in a real metal. Opt. Commun. **239**(1), 61–66 (2004)
9. Estrada, H., Candelas, P., Uris, A., Belmar, F., de Abajo, F.J.G., Meseguer, F.: Extraordinary sound screening in perforated plates. Phys. Rev. Lett. **101**(8), 084302 (2008)
10. Fano, U.: Effects of configuration interaction on intensities and phase shifts. Phys. Rev. **124**(6), 1866 (1961)
11. Fedotov, V.A., Rose, M., Prosvirnin, S.L., Papasimakis, N., Zheludev, N.I.: Sharp trapped-mode resonances in planar metamaterials with a broken structural symmetry. Phys. Rev. Lett. **99**(14), 147401 (2007)
12. Fellay, A., Gagel, F., Maschke, K., Virlouvet, A., Khater, A.: Scattering of vibrational waves in perturbed quasi-one-dimensional multichannel waveguides. Phys. Rev. B **55**(3), 1707 (1997)
13. García-Meca, C., Ortuño, R., Rodríguez-Fortuño, F.J., Martí, J., Martínez, A.: Negative refractive index metamaterials aided by extraordinary optical transmission. Opt. Express **17**(8), 6026–6031 (2009)
14. Garg, J., Bonini, N., Kozinsky, B., Marzari, N.: Role of disorder and anharmonicity in the thermal conductivity of silicon-germanium alloys: A first-principles study. Phys. Rev. Lett. **106**(4), 045901 (2011)
15. Han, H., Li, B., Volz, S., Kosevich, Yu.A.: Ultracompact interference phonon nanocapacitor for storage and lasing of coherent terahertz lattice waves. Phys. Rev. Lett. **114**(14), 145501 (2015)
16. Han, H., Potyomina, L.G., Darinskii, A.N., Volz, S., Kosevich, Yu.A.: Phonon interference and thermal conductance reduction in atomic-scale metamaterials. Phys. Rev. B **89**(18), 180301 (2014)
17. Han, T., Bai, X., Gao, D., Thong, J.T.L., Li, B., Qiu, C.W.: Experimental demonstration of a bilayer thermal cloak. Phys. Rev. Lett. **112**(5), 054302 (2014)
18. Hong, C.K., Ou, Z.Y., Mandel, L.: Measurement of subpicosecond time intervals between two photons by interference. Phys. Rev. Lett. **59**(18), 2044 (1987)
19. Kaburaki, H., Li, J., Yip, S., Kimizuka, H.: Dynamical thermal conductivity of argon crystal. J. Appl. Phys. **102**(4), 043514 (2007)

20. Khalatnikov, I.M.: An Introduction to the Theory of Superfluidity. Westview Press, New York (2000)
21. Kim, W., Zide, J., Gossard, A., Klenov, D., Stemmer, S., Shakouri, A., Majumdar, A.: Thermal conductivity reduction and thermoelectric figure of merit increase by embedding nanoparticles in crystalline semiconductors. Phys. Rev. Lett. **96**(4), 045901 (2006)
22. Kosevich, YuA: Capillary phenomena and macroscopic dynamics of complex two-dimensional defects in crystals. Prog. Surf. Sci. **55**(1), 1–57 (1997)
23. Kosevich, YuA: Multichannel propagation and scattering of phonons and photons in low-dimension nanostructures. Physics-Uspekhi **51**(8), 848–859 (2008)
24. Kosevich, YuA, Feher, A., Syrkin, E.S.: Resonance absorption, reflection, transmission of phonons and heat transfer through interface between two solids. Low Temp. Phys. **34**(7), 575–582 (2008)
25. Kosevich, Yu.A., Gann, V.V.: Magnon localization and Bloch oscillations in finite Heisenberg spin chains in an inhomogeneous magnetic field. J. Phys.-Condens. Mat. **25**(24), 246002 (2013)
26. Kosevich, Yu.A., Syrkin, E.S.: Resonant interaction of elastic waves with a planar crystal defect. Sov. Phys.-Sol. State **33**(7), 1156–1157 (1991)
27. LAMMPS WWW Site: http://lammps.sandia.gov
28. Landau, L.D., Lifshitz, E.M.: Quantum Mechanics (Non-Relativistic Theory). Pergamon Press, Oxford (1991)
29. Lang, C., Eichler, C., Steffen, L., Fink, J.M., Woolley, M.J., Blais, A., Wallraff, A.: Correlations, indistinguishability and entanglement in Hong-Ou-Mandel experiments at microwave frequencies. Nature Phys. **9**(6), 345–348 (2013)
30. Li, N., Ren, J., Wang, L., Zhang, G., Hänggi, P., Li, B.: Phononics: manipulating heat flow with electronic analogs and beyond. Rev. Mod. Phys. **84**(3), 1045 (2012)
31. Liu, N., Liu, H., Zhu, S., Giessen, H.: Stereometamaterials. Nat. Photonics **3**(3), 157–162 (2009)
32. Liu, Z., Zhang, X., Mao, Y., Zhu, Y.Y., Yang, Z., Chan, C.T., Sheng, P.: Locally resonant sonic materials. Science **289**(5485), 1734–1736 (2000)
33. Maldovan, M.: Narrow low-frequency spectrum and heat management by thermocrystals. Phys. Rev. Lett. **110**(2), 025902 (2013)
34. Mingo, N., Hauser, D., Kobayashi, N.P., Plissonnier, M., Shakouri, A.: "Nanoparticle-in-Alloy" approach to efficient thermoelectrics: Silicides in SiGe. Nano Lett. **9**(2), 711–715 (2009)
35. Mitrofanov, O., Lee, M., Hsu, J.M.P., Pfeiffer, L.N., West, K.W., Wynn, J.D., Federici, J.F.: Terahertz pulse propagation through small apertures. Appl. Phys. Lett. **79**(7), 907–909 (2001)
36. Narayana, S., Sato, Y.: Heat flux manipulation with engineered thermal materials. Phys. Rev. Lett. **108**(21), 214303 (2012)
37. Pernot, G., Stoffel, M., Savic, I., Pezzoli, F., Chen, P., Savelli, G., Jacquot, A., Schumann, J., Denker, U., Mönch, I., et al.: Precise control of thermal conductivity at the nanoscale through individual phonon-scattering barriers. Nat. Mater. **9**(6), 491–495 (2010)
38. Plimpton, S.: Fast parallel algorithms for short-range molecular dynamics. J. Comput. Phys. **117**(1), 1–19 (1995). http://lammps.sandia.gov
39. Rubin, R.L., Greer, W.L.: Abnormal lattice thermal conductivity of a one-dimensional, harmonic, isotopically disordered crystal. J. Math. Phys. **12**(8), 1686–1701 (1971)
40. Santori, C., Fattal, D., Vučković, J., Solomon, G.S., Yamamoto, Y.: Indistinguishable photons from a single-photon device. Nature **419**(6907), 594–597 (2002)
41. Savin, A.V., Kosevich, Yu.A.: Thermal conductivity of molecular chains with asymmetric potentials of pair interactions. Phys. Rev. E **89**(3), 032102 (2014)
42. Schelling, P.K., Phillpot, S.R.: Multiscale simulation of phonon transport in superlattices. J. Appl. Phys. **93**(9), 5377–5387 (2003)
43. Schelling, P.K., Phillpot, S.R., Keblinski, P.: Phonon wave-packet dynamics at semiconductor interfaces by molecular-dynamics simulation. Appl. Phys. Lett. **80**(14), 2484–2486 (2002)
44. Stillinger, F.H., Weber, T.A.: Computer simulation of local order in condensed phases of silicon. Phys. Rev. B **31**(8), 5262–5271 (1985)

45. Walia, S., Shah, C.M., Gutruf, P., Nili, H., Chowdhury, D.R., Withayachumnankul, W., Bhaskaran, M., Sriram, S.: Flexible metasurfaces and metamaterials: a review of materials and fabrication processes at micro- and nano-scales. Appl. Phys. Rev. **2**(1), 011303 (2015)
46. Wang, S.M., Mu, S.Y., Zhu, C., Gong, Y.X., Xu, P., Liu, H., Li, T., Zhu, S., Zhang, X.: Hong-Ou-Mandel interference mediated by the magnetic plasmon waves in a three-dimensional optical metamaterial. Opt. Express **20**(5), 5213–5218 (2012)
47. Xu, H., Shi, X., Gao, F., Sun, H., Zhang, B.: Ultrathin three-dimensional thermal cloak. Phys. Rev. Lett. **112**(5), 054301 (2014)
48. Zhang, L., Keblinski, P., Wang, J.S., Li, B.: Interfacial thermal transport in atomic junctions. Phys. Rev. B **83**(6), 064303 (2011)